A multiscale design and fabrication approach to create biomimetic tunable implants using additive manufacturing

Ameen Subhi^{1,2}, Iris X. Quan¹, Liza-Anastasia DiCecco^{1,3*}

- ¹ Department of Systems Design Engineering, University of Waterloo, Waterloo, Ontario, N2L 3G1, Canada
- ² Department of Kinesiology and Health Sciences, University of Waterloo, Waterloo, Ontario, N2L 3G1, Canada
- ³ Waterloo Institute for Nanotechnology, University of Waterloo, Waterloo, Ontario, N2L 3G1, Canada
- * ldicecco@uwaterloo.ca

Abstract: Canadians across the country rely on hard-tissue implants such as hip, knee, and dental implants. Rises in aging populations are further increasing these needs, where diseases prevalent in elderly patients, such as osteoporosis (OP), contribute to these demands and can complicate osseointegration processes. To better serve these populations, current biomaterials used in bone implants must be improved, which can suffer failure from effects such as stress shielding, instability, inflammation, and aseptic loosening. In this work, a multiscale design and manufacturing approach using additive manufacturing (AM) was introduced to design tunable porous scaffolds with biomimetic hierarchical features. For tunable scaffold design, literature-driven design parameters found to be suitable for enhancing osseointegration and appropriate for AM were consulted. A Voronoi tessellation strategy was adopted to create dynamically tunable structures using a parametric modelling approach. In-model topology evaluation metrics (e.g. porosity, strut diameter, node connectivity, and intertrabecular angles) were included to provide designers insight into scaffold mimetics to different bone structures, key for considering site-specific locations and conditions, such as healthy versus OP bone. Current progress related to the materials and mechanical assessment of as-printed scaffold structures is shared. Select scaffold structures were produced using state-of-the-art laser powder bed fusion with Ti-6Al-4V. AM introduced micro-roughness, while chemical etching will induce engineered nanoscale texturing, which is anticipated to improve cellular adhesion and bone growth. Laser profilometry and scanning electron microscopy characterized surface roughness and morphology, while the influence of AM and computer-aided design (CAD) parameters on material properties in future will be assessed in mechanical testing. Overall, this work builds a foundation for the design of innovative biomimetic porous implants that can be tuned to meet patient-specific needs.

Keywords: additive manufacturing, scaffolding, implant, titanium, computer-aided design

1. Introduction

With Canada's aging population, musculoskeletal conditions such as osteoporosis (OP) are expected to rise. OP, characterized by increased bone porosity and reduced strength, is linked to higher rates of implant complications due to stress shielding, instability, inflammation, and aseptic loosening [1–4]. These risks highlight the need for patient-specific implant solutions that mimic native bone to improve osseointegration in compromised conditions. Voronoi tessellation enables scaffold designs that replicate the porosity and anisotropy of trabecular bone, supporting bone regeneration and vascularization [5,6]. Voronoi scaffolds can be engineered with reduced stiffness to mitigate stress shielding and tuned to match bone site conditions e.g., healthy, OP. Due to their geometric complexity, additive manufacturing (AM), particularly laser powder bed fusion (L-PBF), is a promising fabrication method. However, limited data exist on build fidelity and surface characteristics of such implant structures. This study evaluates the dimensional accuracy and surface roughness of Ti-6Al-4V Voronoi scaffolds produced via L-PBF. Designs of varying porosity were fabricated and chemically etched to increase surface nano-roughness, a factor known to improve osseointegration and bone healing [7].

2. Materials and methods

2.1. Voronoi scaffold design

The Voronoi design was adapted from published parametric models [5,6,8], using Rhinoceros3D V6 (Robert McNeel & Associates, Seattle, USA) with the Grasshopper add-on. Topology and histomorphometry metrics can be adjusted in-model and Strut radii were controlled through approximating Voronoi unit cells to spheres and adjusting size accordingly for each cell. Cylindrical scaffolds with a diameter and height of 8 mm were created, with varying parameters (Table 1).

2.2. Manufacturing

Solid cylindrical platens that were 2 mm in thickness were added to each end of the scaffold to facilitate mechanical testing. Scaffolds were produced through AM via L-PBF, with the circular faces oriented parallel to the build plate. Ti-

6Al-4V grade 23 feedstock powder with particle size 15-45 μm (AP&C, Boisbriand, CAN) was used in an EOS M290 with a spot size of 100 μm (EOS GmbH, Krailing, DEU). Each scaffold was fabricated using the following parameters: laser power of primarily 230-240 W, speed of 900 mm/s, layer thickness of 0.04 mm, and hatch offset of 0.015 mm. Postmanufacturing, implants were ultrasonicated (15 min in ethanol, 15 min in acetone, and 5 min in deionized (DI) water) and acid-etched in 50% v/v sulfuric acid (H_2SO_4), 50% v/v DI water for 2 h to induce surface texturing [9].

TC 1 1 1 D1 '	1 1	C 1 '
Toble Dhyggg	Lohorootorictics	ot decima
Table 1. Physica	I CHALACIELISHICS	OL OESIPHS.
10010 1. 1111 010.		01 000151101

Design	Seeds/Plane	Approx. Strut Radius [mm]	Porosity [%]	Intertrabecular Separation [mm]	Pore Size [mm]
A	16	0.2	78.55	1.42 ± 0.53	0.73 ± 0.58
В	18	0.25	72.63	1.29 ± 0.40	0.62 ± 0.51
C	20	0.3	69.09	1.14 ± 0.41	0.51 ± 0.44

2.3. Characterization

2.3.1. Surface characterization

Laser profilometry was conducted using the Keyence VK-X250 3D Laser Scanning Confocal Microscope (Keyence, Osaka, JPN). Surface roughness was measured using the Keyence Multi-file Analysis Application (Keyence, Osaka, JPN). Images were taken using the Hitachi SU8700 (Hitachi, Tokyo, JPN) scanning electron microscope (SEM). Samples were mounted on 6 mm stubs and secured using carbon tape, copper tape, and silver colloidal adhesive. The samples were imaged in secondary electron (SE) mode at 5 kV with a working distance of 6 mm.

2.3.2. Micro-Computer Tomography

High-resolution micro-computer tomography (CT) was conducted for each design with a voxel size of 9 μ m using the Xradia 520 Versa (Zeiss, Oberkochen, DEU), where geometric fidelity and build-porosity were assessed using Dragonfly (V. 1.30.3, Object Research Systems, Montréal, CAN) [10]. A cylindrical region of interest (ROI) measuring 7.5 mm in height and 4.5 mm in radius was defined to isolate the Voronoi portion of the scaffold. Designed porosity was calculated by segmenting the material and void volumes within this ROI to determine their relative volume fractions. For internal build pore defect inclusion analysis, only voids exceeding a threshold of 27 voxels (3 × 3 × 3) were considered to exclude segmentation noise. To assess dimensional fidelity, deviation analysis was performed using a contour mesh of the reconstructed volume and registering it to the original computer-aided design (CAD) file using mesh registration and alignment tools. This enabled spatially resolved deviation maps of as-printed geometry vs CAD models.

3. Results and discussion

3.1. Surface characterization

Partially sintered Ti-6Al-4V granules inherent to L-PBF result in scaffold microscale roughness. Etching introduced nanoscale pitting across both partially and fully fused regions, though uneven pitting indicated inconsistent etching, as shown in Figure 1. Arithmetic mean height (Sa) increased from 7.16 ± 0.77 µm to 9.12 ± 0.76 µm and root mean square height (Sq) decreased from 9.12 ± 0.76 µm to 8.48 ± 1.08 µm, indicating minor changes in mean height. However, etching significantly increased the surface area ratio (SA/A) from 1.91 ± 0.14 to 2.12 ± 0.17 and reduced peak defect height.

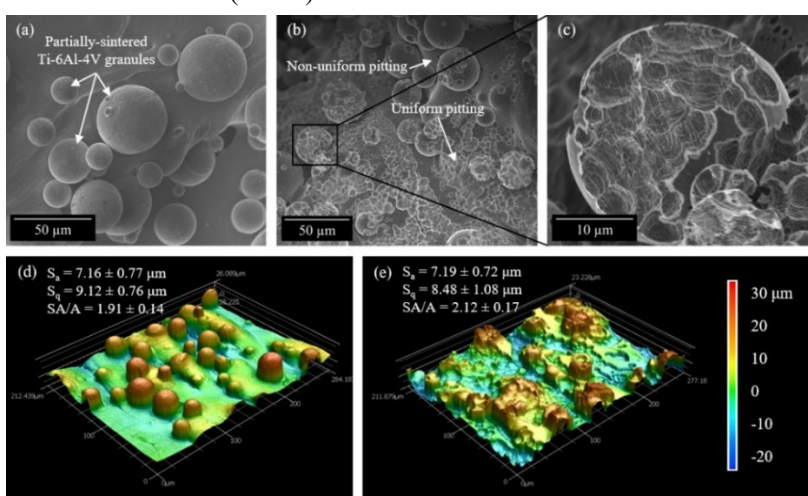


Figure 1. Representative surface characterization of as-printed and etched surfaces. SE SEM micrographs of (a) unetched and (b,c) etched surfaces. Laser profilometry of (d) unetched and (e) etched surface.

3.2. Micro-CT

Micro-CT analysis revealed the bulk design porosity of each scaffold (Figure 2): 71.25% in A, 70.64% in B and 69.94% in C. Deviation heatmaps illustrate the differences in build fidelity among the three designs, revealing that design A had the largest deviation of 7.3% in design porosity, while designs B and C mostly adhered to an ideal range of ± 0.10 mm. Comparing CAD porosity to as-printed porosity for design C suggested that the structure under printed, but further examination of the deviation map and histogram data revealed a slight overprint, with a mean deviation of ± 0.03 mm. However, 90% of deviation values fell within ± 0.05 mm to ± 0.13 mm and did not indicate substantial fidelity issues. In analyzing the internal pore defect inclusions arising from AM, between 70,000 and 100,000 individual internal voids were identified per scaffold. The resulting internal porosity defect values, inversely proportional to fill volume were 0.04 $\pm 0.01\%$ in A, ± 0.006 mean and $\pm 0.01\%$ in B and $\pm 0.01\%$ in C. Defect pore mean aspect ratios were 1.13 (A), 1.36 (B), and 1.11 (C), indicative that voids were predominantly spherical in nature. The mean segment Euclidean lengths, representing the longest internal span across each pore, were 60 $\pm 0.01\%$ m for B, and 50 $\pm 0.01\%$ m for C.

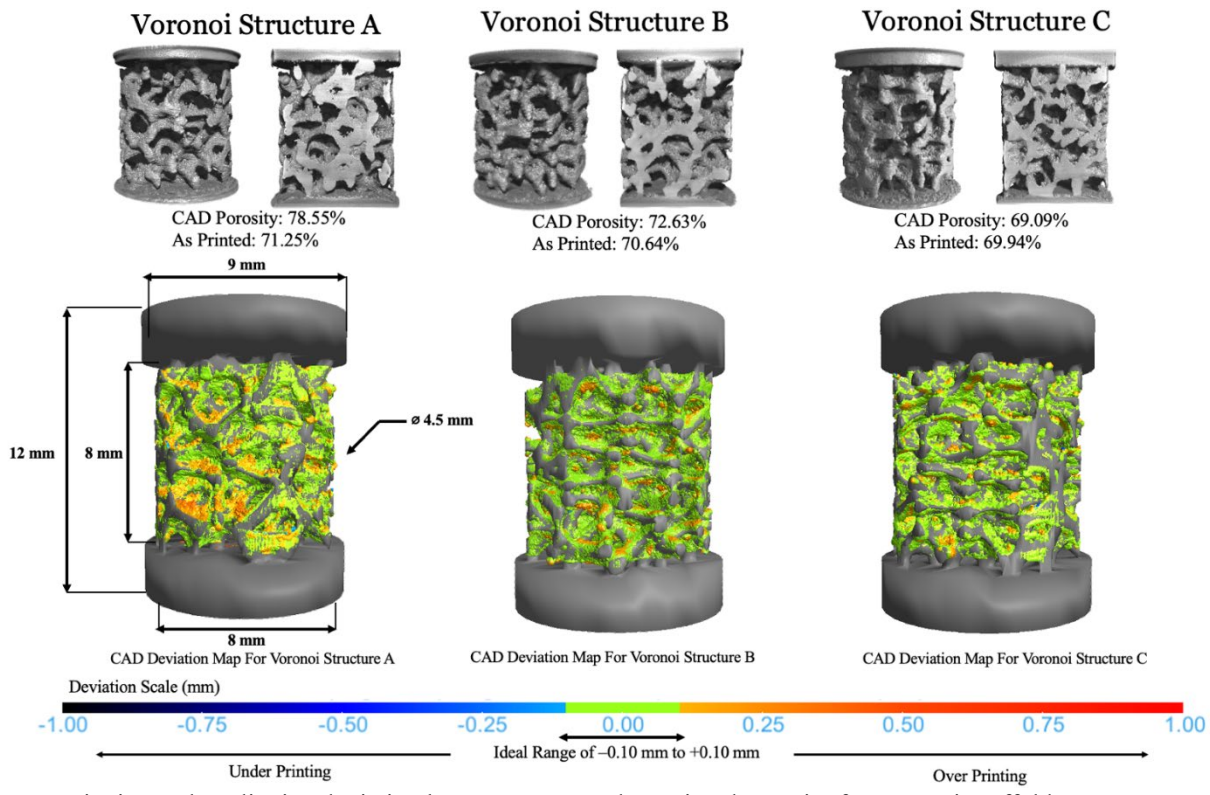


Figure 2. Quantitative and qualitative deviation between CAD and as-printed porosity for Voronoi scaffold structures A, B and C.

3.3. Discussion

Multiscale tunable biomimetic scaffold structures were successfully designed and manufactured through AM. The porosity deviation observed in design A indicates that scaffolds with thinner strut radii are particularly susceptible to build inaccuracies in L-PBF. These inaccuracies arise from AM resolution, specifically the 100 μm resolution of the EOS M 290, which constrains the reliable fabrication of fine lattice features. As strut radii approach the lower bounds of this resolution, geometric fidelity degrades due to over-melting, powder fusion, and unintended strut thickening [11]. Similar findings have been reported using the Renishaw AM400 (77 μm spot size), where struts near 250 μm exhibited dimensional errors between 5% and 25%, while larger struts maintained acceptable dimensional error of 1-4% [12]. In the present study, the ~10% deviation in design A suggests that the thinner struts required for higher porosity scaffolds exceed the process capability of the EOS M 290, with the settings considered. By contrast, designs B and C, which incorporated thicker struts, showed minimal design porosity deviation and closely matched CAD models, indicating that lower-porosity scaffolds fall within the processable resolution range and allow for more controlled material deposition.

Micro-CT analysis of internal inclusion defect porosity revealed no significant variation across the three designs, with volumetric void content ranging from 0.04% to 0.06% with mean Euclidean lengths varying between 50 to 80 μm. The internal pores had more spherical geometries, which are less likely to act as crack initiation sites compared to elongated or irregular voids [13]. Nevertheless, the prevalence of internal pores indicates limitations in L-PBF. Although minor in volume, the concentration of stresses at these internal pores may influence mechanical strength performance.

Chemical etching successfully increased nanoscale surface roughness without significantly altering microscale parameters such as S_a and S_q. However, some partially sintered Ti-6Al-4V granules were not fully removed by the etching process. The persistence of these titanium particles is a clinical concern since particle detachment in vivo may trigger inflammatory responses, osteolysis, or implant loosening [14]. Issues with etching uniformity can be attributed to inconsistent temperature and agitation during the etching process. Chemical etching should be optimized to improve uniformity of nanoscale roughness and eliminate surface defects associated with partially sintered Ti-6Al-4V particles.

4. Conclusion

This study demonstrates that L-PBF can reliably print Voronoi-based Ti-6Al-4V scaffolds with strut radii above 250 µm. Attributed to the 100 µm resolution of the AM systems, scaffolds with a 200 µm exhibited significant overprinting characterized by dimensional errors of ~10% with printing parameters considered. Furthermore, while L-PBF produced internal void defects, micro-CT analysis highlighted that void defects presented limited concern due to their minimal volumetric presence (0.04-0.06%) and predominantly near-spherical shapes, reducing their risk of acting as crack propagation sites. Chemical etching successfully enhanced nanoscale roughness while reducing topological defects from partially sintered granules, which is anticipated to enhance osseointegration in future. These methods enable the design of tunable scaffolds tailored to patient-specific needs, with particular benefit for musculoskeletal diseases such as OP, where porosity can reduce effective Young's Moduli to mitigate bone-implant mechanical mismatch. Next steps include optimizing the chemical etching to improve uniformity and increase removal of residual granules that could pose a threat *in vivo*. Mechanical testing and numerical analysis will be presented at HI-AM to quantify how deviations from the intended CAD geometry impact the mechanical integrity of scaffolds. In summary, this research lays the groundwork for developing innovative biomimetic porous implants that can be tailored to address individual patient needs.

5. Acknowledgments

Financial support provided by the Natural Sciences and Engineering Research Council of Canada (NSERC) (NSERC USRA for IXQ) and funding from the University of Waterloo Start-Up grant program (LAD) are greatly acknowledged. Dr. Sagar Patel from the Multiscale Additive Manufacturing Lab (MSAM) is further acknowledged for his continuous support and help in with Micro-CT analysis.

6. References

- [1] Osteoporosis Canada 2022 Osteoporosis Canada Facts and Stats [Internet]. Osteoporosis Canada; 2022. Available from: https://osteoporosis.ca/facts-and-stats
- [2] Wang CW (Jeff), McCauley LK. Osteoporosis and Periodontitis. Curr Osteoporos Rep. 2016;14(6):284–91.
- [3] Aghaloo T, Pi-Anfruns J, Moshaverinia A, Sim D, Grogan T, Hadaya D. The Effects of Systemic Diseases and Medications on Implant Osseointegration: A Systematic Review. Int J Oral Maxillofac Implant. 2019;34:s35–49.
- [4] Osterhoff G, Morgan EF, Shefelbine SJ, Karim L, McNamara LM, Augat P. Bone mechanical properties and changes with osteoporosis. Injury. 2016;47:S11–20.
- [5] Fantini M, Curto M, Crescenzio FD. A method to design biomimetic scaffolds for bone tissue engineering based on Voronoi lattices. Virtual Phys Prototyp. 2016;11(2):77–90.
- [6] Deering J, Dowling KI, DiCecco LA, McLean GD, Yu B, Grandfield K. Selective Voronoi tessellation as a method to design anisotropic and biomimetic implants. J Mech Behav Biomed Mater. 2021;116:104361.
- [7] Zhang Y, Fan Z, Xing Y, Jia S, Mo Z, Gong H. Effect of microtopography on osseointegration of implantable biomaterials and its modification strategies. Front Bioeng Biotechnol. 2022;10:981062.
- [8] Fantini M, Curto M. Interactive design and manufacturing of a Voronoi-based biomimetic bone scaffold for morphological characterization. Int J Interact Des Manuf (IJIDeM). 2018;12(2):585–96.
- [9] Linn TY, Salamanca E, Ho CY, Wu YF, Chiu HC, Chang WJ, et al. Enhancement of titanium surfaces using different acid solutions at room temperature to improve bone cell responses. J Dent Sci. 2025;20(1):373–83.
- [10] Dragonfly 2024.1 [Internet]. Montreal, Canada: Comet Technologies Canada Inc.; Available from: https://dragonfly.comet.tech/
- [11] Nudelis N, Mayr P. Defect-based analysis of the laser powder bed fusion process using X-ray data. Int J Adv Manuf Technol. 2022;123(9–10):3223–32.
- [12] López-García C, García-López E, Siller HR, Sandoval-Robles JA, Rodriguez CA. A dimensional assessment of small features and lattice structures manufactured by laser powder bed fusion. Prog Addit Manuf. 2022;7(4):751–63.
- [13] Siddharth, Tiwari S, Biswas P, Mandal N, Roy S. Effect of SiC particle size and content on the mechanical and tribological properties of porous Si3N4-SiC composites fabricated following a facile low-temperature processing route. Ceram Int. 2025;51(14):19508–23.
- [14] Zhou Z, Shi Q, Wang J, Chen X, Hao Y, Zhang Y, et al. The unfavorable role of titanium particles released from dental implants. Nanotheranostics. 2021;5(3):321–32.